Acta Biomaterialia 143 (2022) 127–137

Contents lists available at ScienceDirect

Acta Biomaterialia

journal homepage: www.elsevier.com/locate/actbio

Full length article

Experimental and numerical analysis of electroactive characteristics of scleral tissue

Jafar Arash Mehr, Hamed Hatami-Marbini*

Mechanical and Industrial Engineering Department, University of Illinois at Chicago, Chicago, IL USA

ARTICLE INFO

Article history:
Received 10 September 2021
Revised 4 January 2022
Accepted 10 January 2022
Available online 14 January 2022

Keywords:
Sclera
Electroactive hydrogels
Experiments
Chemo-electro-mechanical theoretical model
Finite element analysis

ABSTRACT

The sclera provides mechanical support to retina and protects internal contents of the eye against external injuries. The scleral extracellular matrix is mainly composed of collagen fibers and proteoglycans (PGs). At physiological pH, collagen molecules are neutral but PGs contain negatively charged glycosaminoglycan chains. Thus, the sclera can be considered as a polyelectrolyte hydrogel and is expected to exhibit mechanical response when subjected to electrical stimulations. In this study, we mounted scleral strips, dissected from the posterior part of porcine eyes, at the center of a custom-designed container between two electrodes. The container was filled with NaCl solution and the bending deformation of scleral strips as a function of the applied electric voltage was measured experimentally. It was found that scleral strips reached to an average bending angle of 3°, 10° and 23° when subjected to 5V, 10V, and 15V, respectively. We also created a chemo-electro-mechanical finite element model for simulating the experimental measurements by solving coupled Poisson-Nernst-Plank and equilibrium mechanical field equations. The scleral fixed charge density and modulus of elasticity were found by fitting the experimental data. The ion concentration distribution inside the domain was found numerically and was used to explain the underlying mechanisms for the scleral electroactive response. The numerical simulations were also used to investigate the effects of various parameters such as the electric voltage and fixed charge density on the scleral deformation under an electric field.

Statement of significance

This manuscript investigates the electroactive response of scleral tissue. It demonstrates that the sclera deforms mechanically when subjected to electrical stimulations. A chemo-electro-mechanical model is also presented in order to numerically capture the electromechanical response of the sclera. This numerical model is used to explain the experimental observations by finding the ion distribution inside the tissue under an electric field. This work is significant because it shows that the sclera is an electroactive polyanionic hydrogel and it provides new information about the underlying mechanisms governing its mechanical and electrical properties.

© 2022 Acta Materialia Inc. Published by Elsevier Ltd. All rights reserved.

1. Introduction

The sclera, a dense connective tissue constituting more than 80% of the outer surface of the eyeball, is essential for optical stability of the eye and protects its inner delicate contents from external damages and laceration. The sclera also provides mechanical support to retina and resists deformation caused by internal and external loads during eye movements or fluctuating intraocular pressure (IOP). The scleral extracellular matrix is mainly composed of collagen, elastin, proteoglycans (PGs), and other glycoproteins [1–3]. PGs consist of a core protein to which glycosaminoglycan (GAG) chains are covalently attached. The GAG content of the sclera is between 0.5% and 1% of its dry weight [4]. The western blot analyses and immunohistochemistry have been used to show the presence of lumican, aggrecan, biglycan, and decorin in the human sclera [5,6], which have been suggested to contribute to scleral structural properties. For example, they have been shown to play a role in the increase of scleral rigidity and stiffness with aging [7].

GAGs are important in defining tensile properties of the sclera [8–10]. GAGs draw water into the tissue and subsequently affect the mechanical properties of sclera; tensile and shear properties of ocular tissues, i.e. cornea and sclera, have been shown to de-

* Corresponding author: 2039 Engineering Research Center, 842 West Taylor St, Chicago IL 60607
E-mail address: hatami@uic.edu (H. Hatami-Marbini).

https://doi.org/10.1016/j.actbio.2022.01.017
1742-7061/© 2022 Acta Materialia Inc. Published by Elsevier Ltd. All rights reserved.

pend onhydration [11–14]. GAGs are linear polysaccharides that are negatively charged under physiological conditions. The building blocks of GAGs are an amino sugar (including a sulfate SO_3^-) and an uronic acid (containing a carboxyl COO^-) [15,16]. Chondroitin sulfate, dermatan sulfate, keratan sulfate, and heparin sulfate are among the GAGs that are commonly found in the sclera [17]. It should also be noted that collagen molecules contain both amino NH_3^+ and carboxyl groups COO^- and become positively and negatively charged at low and high pHs, respectively [18,19]. Due to the presence of fixed charges in its extracellular matrix, the sclera is expected to act as a polyanioinic or polycationic hydrogel depending on the pH of the surrounding medium. Under physiological pH, PGs are negatively charged while collagen molecules are neutral [15,20]. Thus, scleral microstructure is similar to that of a natural polyanionic gel and is expected to show an electroactive response [18,19]. The primary objective of the present study is to investigate electromechanical properties of sclera as a biological electroactive hydrogel.

Electroactive hydrogels are important for different applications from robotic and artificial muscles [21,22] to drug delivery systems and actuators [23,24]. These gels transform electrical energy into mechanical work. There exists a vast literature on the deformation of electroactive hydrogels but we here give a brief overview of this broad field; readers are referred to reference [25–28] for more comprehensive review. Hamlen et al.'s work is one of the early studies that showed swelling and shrinking of polyelectrolyte gels in the presence of an electric field [29]. Later, Tanaka et al. determined the reversible volume change of polyelectrolyte gels because of an electric field [30]. The effects of various parameters such as environmental pH, bathing ionic strength, and crosslink density on the swelling and deformation of electroactive hydrogels in response to electrical stimulations have been studied [31,32]. The electro-chemo-mechanical response of collagen membranes as biological polyelectrolytes has also been characterized [33,34]. The contraction and expansion of hydrogels under electrical stimulations is due to electrodiffusion, electroosmosis, and polymer deformation [35,36] as well as the electrophorectic and electro-osmotic transport of ionic species and water molecules [37,38]. The bending of electroactive hydrogels under electrical stimulations is because of the difference in the ion concentration inside and outside of gels [39,40]. A theoretical framework has been developed to express the kinetics of swelling and shrinking in crosslinked polymethacrylic acid hydrogels under chemical and electrical stimulations [41]. Furthermore, a simplified theory for the swelling behavior of ionic gels under an electric field showed that the speed of swelling is proportional to the square of the applied DC current [42]. A chemo-electro-mechanical (CEM) model has also been proposed for predicting the swelling and deswelling rates of hydrogels placed in pH buffer solutions [25,43]. A similar CEM model has been used to show promising microfluidic applications of stimuli-responsive hydrogels in high-speed valves and pumps [44]. The coupled CEM model explained the swelling of ionic polymer gels in terms of concentration differences at the gel–solution interface [45]. The differences in numerical predictions of a fully coupled CEM model and one-way chemo-electric to mechanical coupled models have also been presented [46]. The CEM model has been used for characterizing the nonlinear deformation of a pH-sensitive hydrogel under an externally applied voltage [31,47]. For this purpose, the finite deformation formulation was built into the mechanical equilibrium equations and the Newton–Raphson iteration methodology was used to numerically solve the problem. The present work developed a coupled CEM model for the electroactive response of the sclera.

The sclera can be considered as a biological polyanionic gel because of the microstructure and composition of its extracellular matrix. In spite of significant literature on the structure and mechanical response of the sclera, its electromechanical properties have not been thoroughly investigated. In the present work, we experimentally quantified the electroactive response of the sclera and created a mathematical model that captures the experimental measurements. For this purpose, we first demonstrated that the sclera is an electroactive tissue by measuring its bending response under an external electric field. In addition, we developed and implemented a numerical CEM model using coupled Poisson-Nernst-Plank and equilibrium mechanical field equations. This model was used to obtain the ion concentration distribution inside the domain and explain the experimental measurements. The numerical model was also used to investigate the effects of various parameters on the deformation of the scleral tissue subjected to an electric field.

2. Materials and methods

2.1. Experiments

Intact porcine eyes were obtained from a slaughterhouse and were transferred to the laboratory at 4 °C. Scleral strips of average size of 25mm × 2.5mm (length × width) were dissected from the area close to the optic nerve head in the superior-inferior direction. The strips were dried in a desiccator for 24 hours in order to obtain their dry weight, W_d. The dried strips were put in 0.15M NaCl solution to swell and their wet weight, W_s, was measured at different time intervals using a digital scale (Mettler-Toledo, OH, USA) with 0.1 mg accuracy. The swelling ratio (S.R) was defined as $(W_s-W_d)/W_d$ and the strips were allowed to swell until their S.R was about 2.0, which was their swelling ratio right after dissection [13]. After measuring the thickness of specimens using a pachymeter (DGH 555B - Exton, PA, USA), they were mounted at the center of a custom-designed container between two carbon electrodes, 5 cm apart from each other, Fig. 1. The scleral samples were fixed from the end closer to superior side while the other end was free to move; the free end was colored with red dye prior to mounting the samples in the testing device. The chamber was filled with 0.15M NaCl solution and the two carbon electrodes were connected to a DC current power supply (BK precision – CA, USA). A digital microscope camera (Koolertron-Shenzhen, China) recorded the bending deformation of samples as a function of time. A Python program tracked the movement of the red colored free end and gave the bending angle of the strips. The bending angle was defined as the deviation of tip of the samples with respect to their initial straight state when no electric field existed, Fig. 1. A total of eighteen scleral strips were used to investigate the bending deformation at three electric potentials of 5V, 10V, and 15V.

We performed additional experiments to determine the speed of pH waves in our experimental setup. Upon applying the voltage, the following chemical reactions occur near the electrodes [48]:

$$\begin{aligned} &2H_2O + 2e^- \rightarrow H_2 + 2OH^- \quad \text{(cathode)} \\ &6H_2O \rightarrow O_2 + 4H_3O^+ + 4e^- \quad \text{(anode)} \end{aligned} \tag{1}$$

These reactions generate two pH waves that propagate from electrodes. It has been previously shown that the pH wave propagation could affect the outcome of electro-actuation experiments [48–51]. The pH waves propagate with a velocity proportional to the magnitude of the applied voltage and specific physical properties of the experimental setup. We hypothesized that any change in the local pH of scleral strips would affect their net fixed charge density (this issue will be discussed later in this work). Thus, we used universal pH indicators (Bogen's Universal pH Indicator Solution) to visualize the propagation of hydronium and hydroxide ions inside the testing chamber when the electric potential was applied. This was done in order to obtain an estimate for the time that it took for the pH waves to reach scleral strips and subse-

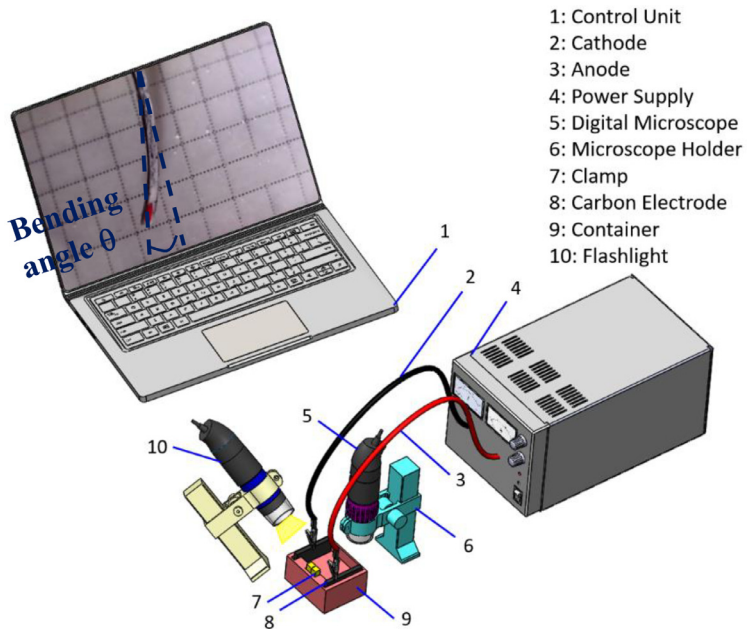

Fig. 1. A schematic plot showing main parts of the experimental device. The observed bending deformation of a typical scleral strip is also shown. The bending angle θ is the amount that the line connecting two end points of a sample rotates in response to an electric field.

quently affect the neutral pH of the solution. The duration of our experiments, i.e. 60 s, was selected based on these measurements.

2.1.1. Statistical analysis

One-way analysis of variance (ANOVA) was used to quantify the effect of voltage on the bending angle of scleral strips. The level of statistical significance was 0.05 in all statistical analyses. Data are presented as mean ± standard deviation.

2.2. Numerical model

We used a coupled chemo-electro-mechanical model based on the nonlinear coupled Poisson-Nernst-Planck (PNP) system for numerical representation of experimental measurements. The Nernst-Planck equation expresses the diffusion, convection, and migration of charged particles and is given by

$$\frac{\partial c_i}{\partial t} + \nabla.(-D_i\nabla c_i - z_i\mu_i F c_i \nabla\phi) = 0, \quad i = Na^+, Cl^-, \tag{2}$$

where ϕ is the electric potential, c_i is the concentration of Na^+ and Cl^- mobile species, D_i is diffusion constant of mobile species, $\mu_i = D_i/RT$ is their mobility, R = 8.3143 J/mol.K is universal gas constant, T is temperature, and F = 96487 C/mol is Faraday constant. Furthermore, the Poisson equation describes the electric field distribution inside a polyelectrolyte and is given by

$$\nabla^2\phi = -\frac{F}{\varepsilon_0\varepsilon_r}(z_{Na^+}c_{Na^+} + z_{Cl^-}c_{Cl^-} + z_{Fixed}c_{Fixed}), \tag{3}$$

where $\varepsilon_0 = 8.85\text{x}10^{-12}$ F/m is the vacuum permittivity, ε_r is the relative permittivity, c_{Fixed} is the concentration of fixed charges, $z_{Na+} = 1$, $z_{Cl^-} = -1$, and $z_{Fixed} = -1$ are the valence of sodium cation, chloride anion, and fixed charges, respectively. The weak forms of Eqs. (2)-(3) become as

$$\begin{gathered}\int_\Omega v_c\frac{\partial c_i}{\partial t}\,dx + \int_\Omega D\nabla c_i.\nabla v_c dx + \int_\Omega \mu_i F c_i z_i \nabla\phi.\nabla v_c\,dx = 0, \quad i = Na^+, Cl^- \\ \varepsilon_0\,\varepsilon_r\int_\Omega \nabla v_\varphi.\nabla\phi\,dx - F\int_\Omega v_\varphi(z_{Na^+}c_{Na^+} + z_{Cl^-}c_{Cl^-} + z_{Fixed}c_{Fixed})dx = 0\end{gathered}, \tag{4}$$

where v_c and v_ϕ are the test functions. We discretized the above PNP system in time using backward Euler method and linearized it before writing its spatial discretization [52–56]. Moreover, the equation of equilibrium for the mechanical field is given by

$$\begin{gathered}\nabla.\boldsymbol{\sigma} + \mathbf{b} = \frac{\partial^2\mathbf{u}}{\partial t^2} \\ \mathbf{b} = \nabla P,\ P = \Delta\tilde{\pi}_2 - \Delta\tilde{\pi}_1\end{gathered}, \tag{5}$$

where $\boldsymbol{\sigma} = (\sigma_{xx}, \sigma_{yy}, \sigma_{xy})^T$ is the stress, $\mathbf{u} = (u_x,u_y)^T$ is the displacement vector, $\mathbf{b} = (b_x,b_y)^T$ represents the body force, and P is the difference between differential normalized osmotic pressure, $\Delta\tilde{\pi}_1$ and $\Delta\tilde{\pi}_2$, at the vicinity of anode side and cathode side of scleral strips, respectively [51]. The normalized differential osmotic pressure $\Delta\tilde{\pi}$ across the boundary of the domain is given by [39, 42–46]:

$$\Delta\pi = RT\sum_{i=Cl^-,Na^+}\left[(c_i)_{inside} - (c_i)_{solution}\right], \quad \tilde{\pi} = \frac{\pi}{RT}, \tag{6}$$

It is noted that $b_y \approx 0$ because of negligible variation in the concentration of mobile species in y-direction (Fig. 2). We used the linear elastic constitutive relation to relate the stress and strain vectors,

$$\begin{pmatrix}\sigma_{xx}\\ \sigma_{yy}\\ \sigma_{xy}\end{pmatrix} = \frac{E}{1-\nu^2}\begin{pmatrix}1 & \nu & 0\\ \nu & 1 & 0\\ 0 & 0 & (1-\nu)/2\end{pmatrix}\begin{pmatrix}\varepsilon_{xx}\\ \varepsilon_{yy}\\ \varepsilon_{xy}\end{pmatrix}, \tag{7}$$

The weak form of the mechanical equation of equilibrium was found after writing the right-hand side of the Eq. (5) as:

$$\frac{\partial^2 u_i}{\partial t^2} = \frac{u_i^n - 2u_i^{n-1} + u_i^{n-2}}{\Delta t^2}, \quad i = x, y, \tag{8}$$

where u_i^k are displacements at discretized time step k and Δt is the length of the time step. The resulting coupled equations were implemented in FEniCS and the chemical, electrical and mechanical fields were found at each time step [56]. For this purpose and considering the experimental set-up (Fig. 2), we considered a 2D domain composed of the NaCl solution, $\Omega_{solution}$, and scleral strips, Ω_{sclera}, Fig. 2. Linear and second order Lagrange elements were used for solving electrochemical fields and the mechanical fields, respectively. On average about 22922 and 1200 finite elements

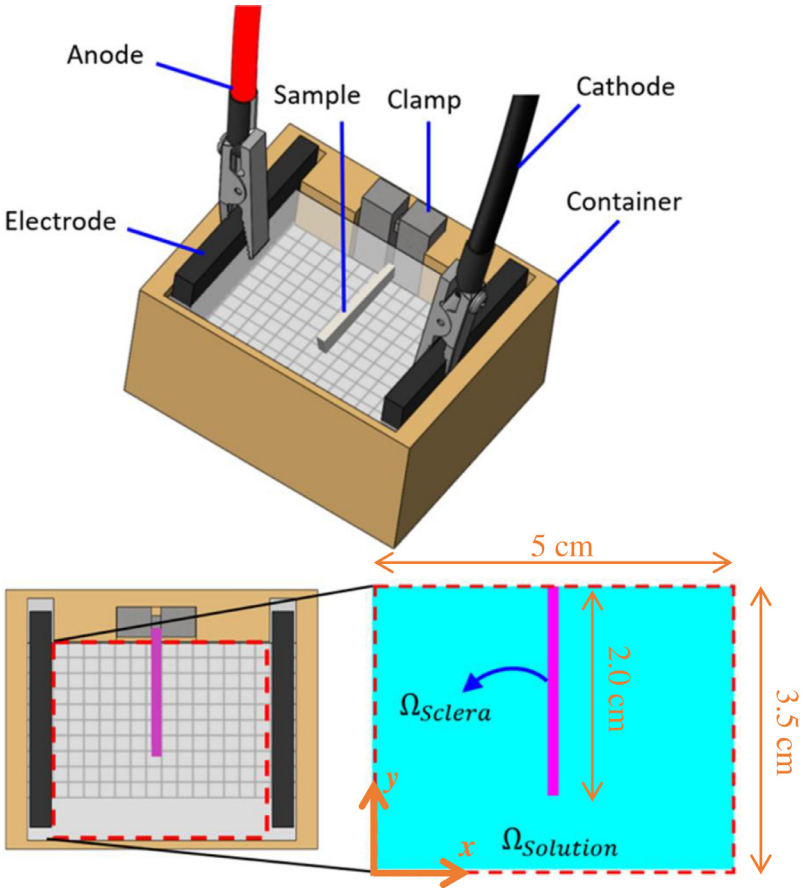

Fig. 2. Schematic 3D illustration of the experimental setup and the 2D domain considered in the numerical studies.

were used in the solution domain and scleral domain, respectively. The mesh was significantly refined at the sclera-solution interfaces in order to be able to capture the steep gradient of the mobile ion concentrations (Appendix B). In addition, we implemented mesh convergence analysis to make sure that numerical results were independent of the number of elements (Appendix B). In the simulations, we took $\Delta t = 0.01$s, $T = 293$ K, $\varepsilon_r = 75$, $D_{Na+} = 1.16\times10^{-9}$ m^2/s, and $D_{Cl^-} = 1.6\times10^{-9}$ m^2/s [57,58]. Furthermore, we applied an electric potential of $\phi = +\phi_0$ at the anode and $\phi = -\phi_0$ at the cathode (ϕ_0 = 2.5, 5, and 7.5 V in different analyses). At the top boundary of the scleral domain where samples were clamped, we enforced $u_x = u_y = 0$. The initial conditions for mobile ion concentrations were $c_{Na+} = c_{Cl^-} = 150$ mol/m^3 in Ω_{sol}. The concentration of mobile ions inside the sclera domain was obtained from the Donnan equation [57,59],

$$(c_{Na^+})_{sclera} = \frac{c_{fixed}+\sqrt{c_{fixed}^2+4(c_{Na^+})_{sol}}}{2}, \qquad (c_{Cl^-})_{sclera} = \frac{-c_{fixed}+\sqrt{c_{fixed}^2+4(c_{Cl^-})_{sol}}}{2} \qquad (9)$$

3. Results and discussion

The average thickness of porcine posterior scleral samples at the beginning of the experiments (S.R = 2.0) was 1.3 mm, which is comparable with what has been previously reported [13,60]. No noticeable difference in the weight and thickness of the strips was observed after experiments were completed. The local pH gradient, which is attributed to water electrolysis, significantly changes the concentration of fixed charges by protonation or deprotonation reactions and could thus influence the bending behavior of electroactive hydrogels [50]. Fig. 3 illustrates the propagation of the pH waves in 0.15M NaCl solution under 15 V at different times. This plot shows that pH waves propagating from the cathode and anode after 120 s of actuation were almost 20 mm and 15 mm

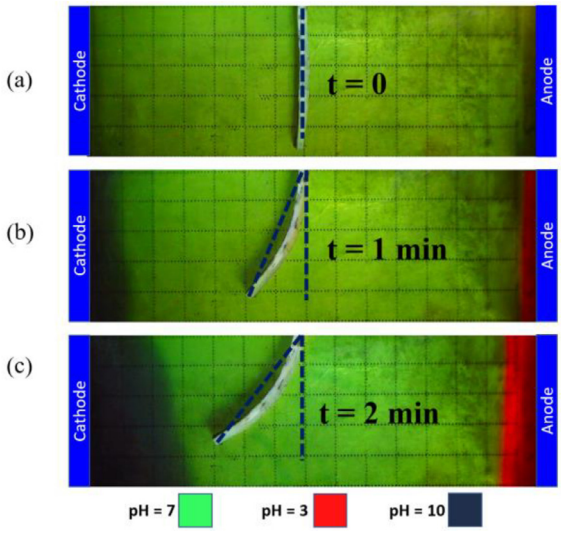

Fig. 3. Propagation of pH waves from the electrodes under 15 V in 0.15M NaCl solution at time a) zero, (b), after 1 minute, and (c) after 2 minutes of the electrical stimulation. The green area corresponds to the neutral medium (pH ≅ 7.0) while the red and dark regions show the acidic (pH < 3.0) and basic (pH > 10.0) regions.

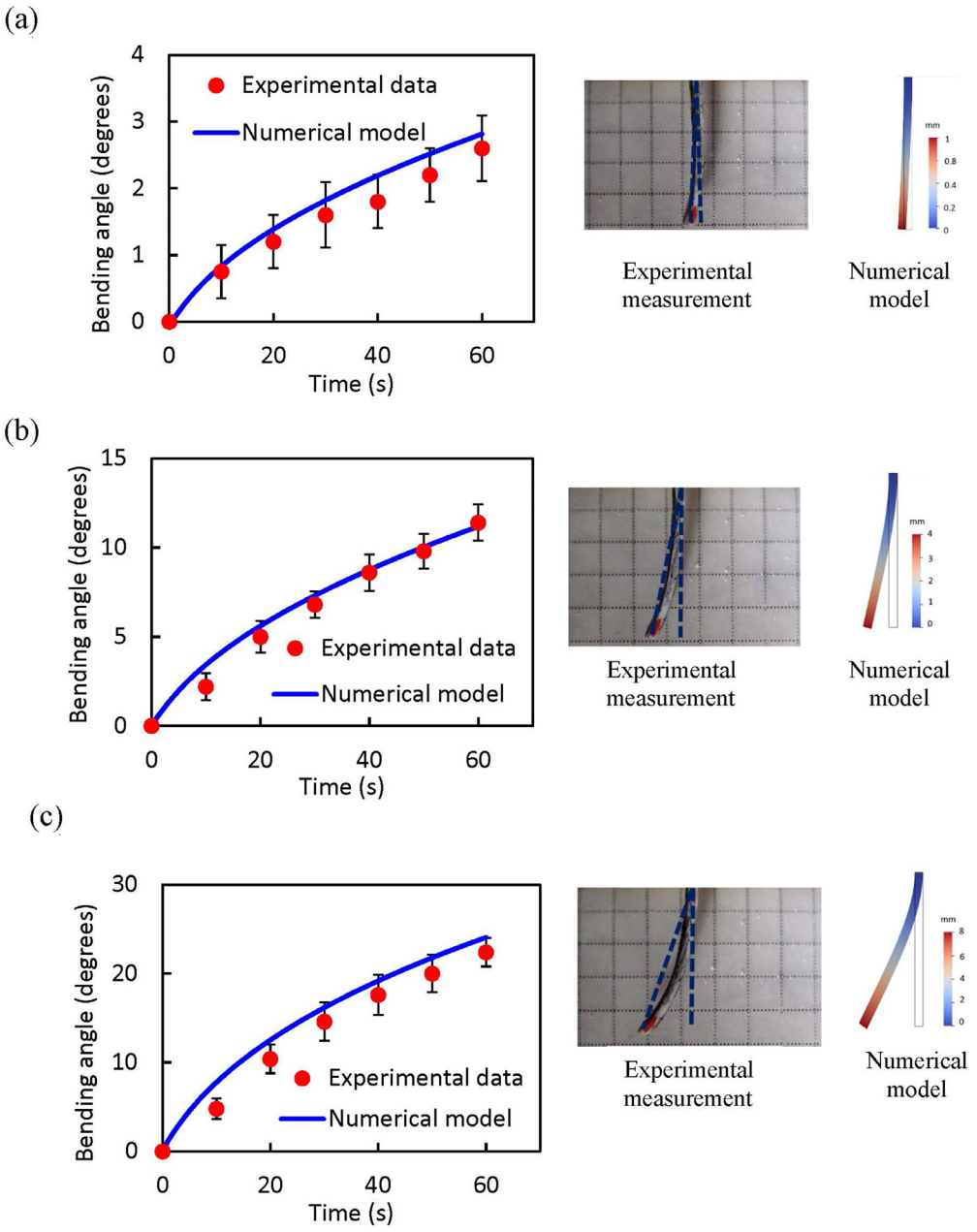

Fig. 4. The bending angle of scleral strips in 0.15M NaCl solution under (a) 5V, (b) 10V, and (c) 15V as a function of time. The symbols and solid lines represent the experimental data and numerical model predictions, respectively. The actual maximum bendings of a representative scleral strip along with their respective numerical model analyses are also shown at each voltage. The bending angle is defined as the angle between the dashed lines.

away from the center of the setup, where the samples were placed, respectively. It is noted that hydroxide ions propagated faster compared to hydronium ions, which is in agreement with a previous study [48]. This observation confirmed that pH waves did not reach scleral strips after 1 minute of electrical stimulation. We presented the bending angle of the sclera within 60 s of electrical actuation to be sure that the generation of pH gradient, due to chemical reactions occurring at the electrodes, did not affect our experimental measurements.

Fig. 4 shows the bending angle of scleral strips for the first 60 seconds of being subjected to 5V, 10V, and 15V. The bending angle of scleral strips gradually increased with time and its magnitude was a function of the applied voltage. There was a significant difference between the maximum bending angle that was observed at 5V, 10V, and 15V. The scleral tissue in neutral pH behaves as a polyanionic hydrogel, which is because of the presence of negative fixed charges in its extracellular matrix, i.e. SO_3^- (in GAGs) and COO^- (in both GAGs and collagen). The pKs of sulfate and carboxyl anions are at pH $\approx$ 2.0 and pH $\approx$ 3.0, respectively [15]. In addition, collagen contains amino groups with pK $\approx$ 8.5 so cations will be formed via protonation if pH $<$ 8.5. In other words, collagen molecules carry both positive and negative charges, which cancel each other at pH $\approx$ 7.0 and subsequently results in a zero net electric charge. However, collagen molecules become charged at non-physiological pH. The total net charge of the scleral tissue is expected to be negative at pH $>$ 10.0 [15,18-20].

We observed that scleral strips, under the applied electric field, bent towards the cathode, proving that the sclera is electro-

responsive. This behavior can be explained in terms of the migration of mobile ion species. The scleral strips include negative fixed charges that cannot move as they are bound to PGs and collagen network. However, because of the application of electric potential, free Na^+ and Cl^- ions inside the solution move towards their counter-electrodes causing a gradient in the osmotic pressure at the boundaries of scleral strips and NaCl solution. In particular, because of the ion migration, the osmotic pressure increases at the boundary close to the anode side while it decreases at the boundary near the cathode side. The resulting osmotic pressure difference within the tissue acts as a driving force bending the strips towards the cathode, which we quantified in our experiments [49,61].

We can also explain the bending behavior of the sclera based on the ion depletion theory [62–64]. According to this theory, the external electric field causes an electric current, because of movement of sodium cations, to pass through any polyanionic hydrogel that is immersed in NaCl solution. This current leads to reduction (depletion) of Na^+ ions near the side of the samples that is close to the anode. At this location, the Cl^- ion concentration decreases in order to satisfy the electro-neutrality condition. Furthermore, the formation of the electric current causes mobile ion concentrations to increase on the opposite side of the samples. Thus, the anode side of the samples swells more compared to their cathode side resulting in their bending towards the negative electrode, i.e. cathode, which was observed in the experimental measurements of the present work.

The proposed numerical model can be used to represent the experimental data shown in Fig. 4. We first validated this model against a previous study in the literature (Appendix A). Except for the scleral Young's modulus E and the amount of fixed charge density c_{Fixed}, all other parameters of the numerical model were assumed to be known and were obtained from the literature, Section 2.2. The Poisson's ratio of 0.48 was taken for the sclera [65]. We found $c_{Fixed} = 10$ mM and $E = 0.2$ MPa from fitting the numerical model to the experimental data. The exact amount of negative charges in the sclera has not yet been determined. However, previous studies estimated $c_{Fixed} = 40$ mM for the corneal tissue at pH = 7.0 [66]. Furthermore, it has been reported that scleral GAG content is about 20-30% of that of the cornea [19,67,68]. Thus, our estimate for the fixed negative charges, i.e., 10 mM, is within the expected range for the scleral tissue. In addition, the Young's modulus of 0.2 MPa is comparable with previous reports for the scleral modulus of elasticity [13,69,70]. Similar to the behavior of any electroactive polyanionic hydrogel, the bending angle of scleral strips depends on the applied voltage. Fig. 4 shows that the chemo-electro-mechanical model was able to capture the experimental measurements at different voltages. It is noted that the same model parameters used for experiments performed at 5 V were used to estimate numerically bending angles under 10 V and 15 V. The fact that the numerical model gave a very good representation of the experiments performed at a different voltage further validates the proposed numerical model.

The increase in the amount of bending angles with increasing the electric potential can be explained by either one of the mechanisms that were discussed earlier for the bending of scleral tissue under the electric potential. With increasing the electric potential, the speed of free mobile ion movement increases and the sclera bends quicker. Fig. 4 shows that it took 60 s and 20 s to obtain a bending angle of ~12° under the electric potential of 10 V and 15 V, respectively. As the voltage increases, more reduction of Na^+ ions occurs near the anode side of scleral strips and the required differential osmotic pressure is generated faster at the scleral strip and solution interface. In general, the electric field provides the required energy for bending the polyelectrolyte gels; thus, the amount of deformation significantly depends on the strength of the electric field [32,51,61,71]. It is noted that we did not observe a considerable bending angle after 60 s under 5 V. However, a measurable bending angle was observed when we subjected the samples to 5 V for a longer period of time. However, we herein presented the experimental results only for 60 s in order to be able to rule out any possible effect of the generated pH gradient on the measurements.

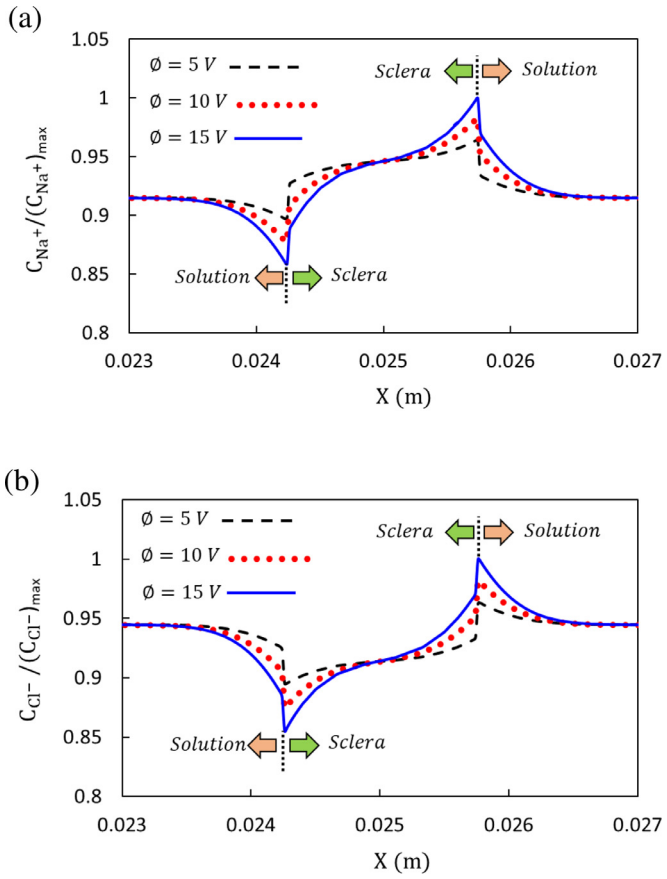

Fig. 5. Effect of voltage on the normalized concentration distribution of (a) sodium, and (b) chloride ions 60 s after electrical actuation. The data is obtained along the line y = 3.0 cm. $(C_{Cl^-})_{max}$ and $(C_{Na^+})_{max}$ denote the maximum concentration of chloride and sodium ions, respectively.

The present numerical model can be used to determine the ion distribution in the scleral strips and their surrounding solution. For example, Fig. 5 shows the normalized concentration of Na^+ and Cl^- ions 60 s after the application of the electric potential at three different voltages. This plot shows the variation of ion concentrations at y = 3.0 cm and along x-direction within the range of 2.435 cm ≤ x ≤ 2.565 cm. Due to the dimensions of scleral samples and the specific experimental setup that we used, the gradient of mobile ions concentrations in the y-direction is negligible [72]. Fig. 5 confirms that the concentrations of mobile species (Na^+ and Cl^-) remained constant and showed little variation far from the boundaries of scleral strips. However, large variations existed near the sclera and solution domain boundaries. This observation is compatible with the proposed mechanism for the scleral bending as outlined above, i.e. the scleral bending is because of changes in chemical concentrations of the free ions. With increasing the voltage, the change in concentrations increases causing larger deformation. Fig. 6 shows the concentration variation at y = 3.0 cm and at 10 V as a function of time. The concentration of Na^+ and Cl^- decreases constantly in the vicinity of sclera and solution boundary facing the anode and increases steadily along the

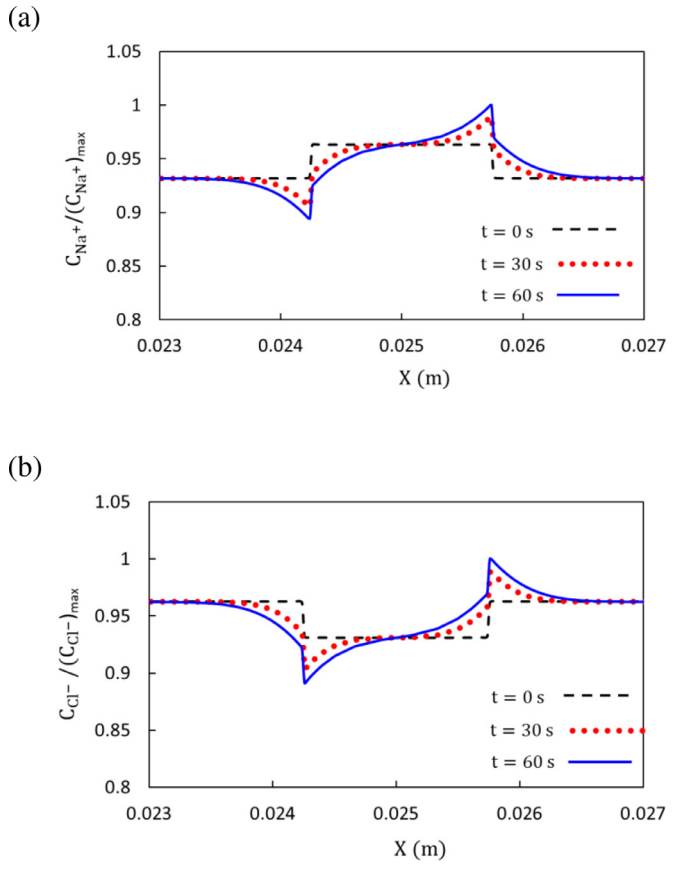

Fig. 6. (a) Sodium cation and (b) chloride anion normalized concentration after the samples were subjected to 10 V for 0, 30s, 60s. The data along the line y = 3.0 cm is shown. $(C_{Cl^-})_{max}$ and $(C_{Na^+})_{max}$ denote the maximum concentration of chloride and sodium ions, respectively.

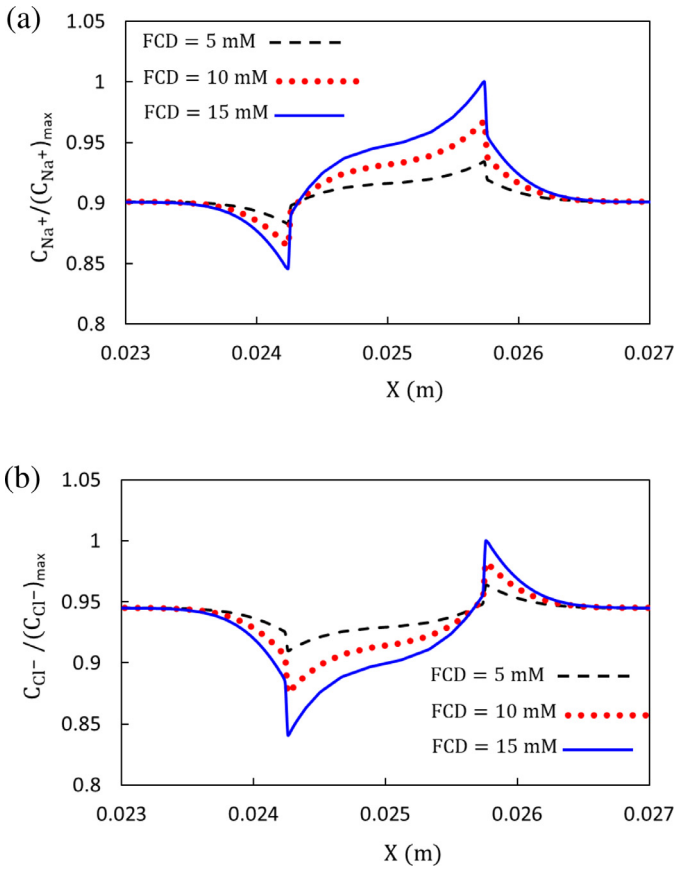

Fig. 7. Effect of fixed charge density (FCD) on the normalized distribution of (a) sodium, and (b) chloride ions 60 s after applying 10V. The data is obtained along the line y = 3.0 cm. $(C_{Cl^-})_{max}$ and $(C_{Na^+})_{max}$ denote the maximum concentration of chloride and sodium ions, respectively.

boundary facing the cathode. The density of fixed negative charges inside scleral strips significantly affects the variation of ion concentration when subjected to an electric field, Fig. 7. The numerical results shown in Figs. 5-7 suggest that any alteration in the applied electric field, the period of stimulation, and fixed charge density have significant influence on the ion concentration distribution at the sclera and solution interface, which in turn affects the amount of scleral bending. In summary, the step-shaped distribution of the mobile ion concentration along x-direction before applying the electric voltage [45,72,73] would change significantly upon applying the voltage, and the ion concentration decreases continuously with time at the anode side and increases at the cathode side, Figs. 5-7. This is in agreement with the theory of depletion polarization and previous studies on polyelectrolyte hydrogels [62,74].

Although not investigated in the present work, the S.R of samples is expected to play a key role in the bending behavior of scleral strips. The FCD inside the sclera could vary as a function of swelling ratio. Furthermore, we have recently shown that S.R has a significant effect on the mechanical response (e.g., Young's modulus) of the sclera [13]. For example, the present numerical model predicts that bending angles decrease with increasing the Young's modulus when scleral strips are subjected to electric potential of 10 V for 10 s. We conducted the experiments at S.R = 2.0; which is the swelling ratio of posterior sclera at physiological conditions and immediately after dissection [13,60,75]. The present work can be extended in future to investigate the effect of hydration on the electroactive response of the scleral tissue. Furthermore, we conducted our experiments in only NaCl solution and such that the pH of the solution surrounding the strips stays constant and equal to 7.0. Any variation in the pH of solution is expected to affect the fixed charge density inside the tissue [15,18-20,66] and makes it difficult to interpret the experimental measurements. The electroactive response of sclera in physiologically relevant solutions such as simulated body fluid (SBF) and OBSS should be investigated in future. In such studies, the numerical model is required to be extended such that it could capture the effects of the electric field on the concentration distribution of different ions that are present in these solutions.

It is noted that the present numerical model does not consider pH dependent variation of fixed charge density inside the samples. For the current experimental set-up, where the maximum electric potential is 15 V and electrodes are 5 cm apart, the present numerical model can be used with confidence when the duration of experiments is about 60 s. This is because it takes more than 60 s for the pH waves to reach the scleral region. If pH waves penetrate the tissue, they could directly affect the concentration of fixed charges because any pH variation causes deprotonation of carboxylic acids, formation of additional carboxyl anions, and/or protonation of NH_3^+ cations into the amine groups; all of which will affect the FCD by changing the existing balance between COO^- and NH_3^+ at pH = 7.0. As a matter of fact, we note here the scleral tissue has an isoelectric point around pH ≈ 4.0 [19,66]. This means that the net charge of the sclera becomes positive below the isoelectric point, i.e., similar to the behavior of polycationic hydrogels, the sclera is expected to bend towards the anode when subjected

to electric potential when pH $<$ 4.0. The present technique can be used to investigate the electroactive response of scleral samples at different pH levels by using pH buffer solutions without being worried about the propagation of pH waves [32,51]. Such pH buffer solutions were not used in the present work since they include many ions making the development of the numerical model and interpretation of the measurements more difficult. Temperature could also be important in determining the bending of sclera when subjected to electric potential. We performed all experiments at room temperature and kept track of temperature using a thermometer (OMEGA – CT, USA). Almost no temperature change was observed when the samples were subjected to electric potential for 60 s. However, we observed that the temperature of the solution would rise when an electric stimulation of 15 V was applied for more than 5 minutes. Finally, it is noted that a 2D linear elastic material model was employed in this study as it was a first-pass effort. Sclera is a fibrous tissue and orientation of collagen fibers is expected to play an important role in its mechanical response [76,77]. We are currently working on extending the present model to a 3D nonlinear hyperelastic material model with consideration of collagen fibers in order to investigate the electroactive response of sclera from different regions of the eye.

4. Conclusions and future work

We presented our findings of an experimental and numerical investigation for the electroactive behavior of the sclera. The scleral strips deformed mechanically when they were subjected to electrical stimulations; thus, we concluded that sclera is an electroactive bio-hydrogel. Specifically, we found that scleral strips reached to an average bending angle of 3°, 10° and 23° after being subjected for 60 seconds to 5V, 10V, and 15V, respectively. All experiments of the present work were performed at pH of 7 and in a saline solution to simplify numerical modelling of the experimental measurements. In future, the effects of solutions such as PBS, OBBS, and SBF on the electromechanical response of the sclera should be investigated. In order to keep the pH constant, we selected the duration of electrical simulations such that pH waves do not reach the sample. This limited our ability to characterize the long-term behavior of sclera when subjected to an electrical field. However, we observed that the rate of deformation of the sclera in response to the electrical stimulations decreases with increasing time. Future work is required to characterize long term response of the sclera by using buffer solution as well as to determine the possible effects of the pH on the electroactive response of the sclera. A numerical chemo-electro-mechanical model was also created. After validating the numerical model against previous numerical model, we calibrated it against our experimental data and investigated numerically the effects of the FCD, applied voltage, and Young's modulus on the bending behavior of the scleral tissue. This numerical model was also used to explain the experimental findings in terms of the ion concentration and electric potential distribution inside the sclera and solution. For example, we proposed that the mechanical bending response of scleral strips is because the external electric potential creates differential osmotic pressure at the cathode and anode sides of the samples. The findings of the present work are important for both biomechanical and biochemical characterizations of the scleral tissue and could have important implications for the future efforts in the field. For example, alterations in scleral GAG content and its subsequent changes in the FCD may cause eye-related disorders; an example is tumor extension in melanoma where GAG accumulation has been proposed to be a contributing factor [78]. Furthermore, myopia is believed to be accompanied by a reduction in the GAG content of the sclera [79]. The proposed method can be used for estimating the negative fixed charges of sclera as well as other electroactive biological tissue. In this first study, we demonstrated the electro-responsiveness of the sclera tissue both experimentally and numerically. However, many questions remain unanswered about the influence of electrical stimulations of the sclera in vivo and future studies are required to determine whether electrically-assisted deformation could safely be induced to the sclera in vivo.

Declaration of Competing Interest

The authors declare that they have no known competing financial interests or personal relationships that could have appeared to influence the work reported in this paper.

Acknowledgement

The authors would like to acknowledge the support in part by National Science Foundation: Grant No. 1635290.

Appendix A

We validated our numerical implementation using a previous study by Wallmersperger et al. [45]. To this end, we used the same geometry that these investigators used: a 5cm $\times$ 5cm solution bath with a 4 mm $\times$ 10 mm gel domain at its center. The solution has

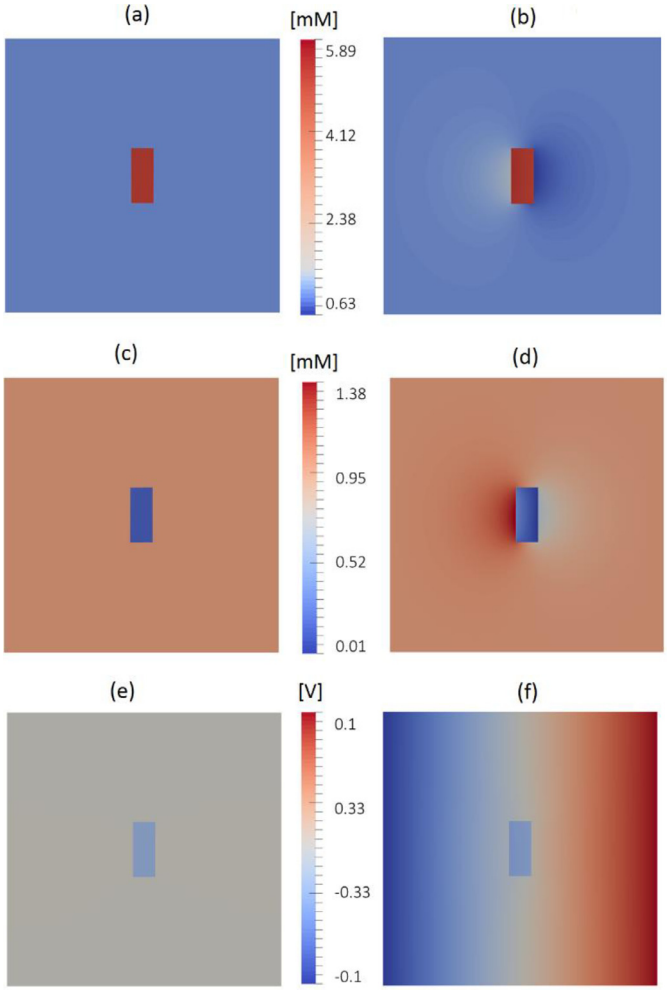

Fig. A.1. The distribution of c_{Na+} in both (a) initial and (b) stationary state. The distribution of c_{Cl-} in both (c) initial and (d) stationary states. The electric voltage distribution over the domain (e) before and (f) after application of the electric voltage.

Table A1
Parameters of the numerical model [45].

Parameters	F	ε_0	ε_r	R	T	D_{Na^+}	D_{Cl^-}
value	96487 $\frac{c}{mol}$	8.85×10^{-12} $\frac{F}{m}$	100	8.3114 $\frac{J}{mol.K}$	293 K	1.0×10^{-7} $\frac{m^2}{s}$	1.0×10^{-7} $\frac{m^2}{s}$

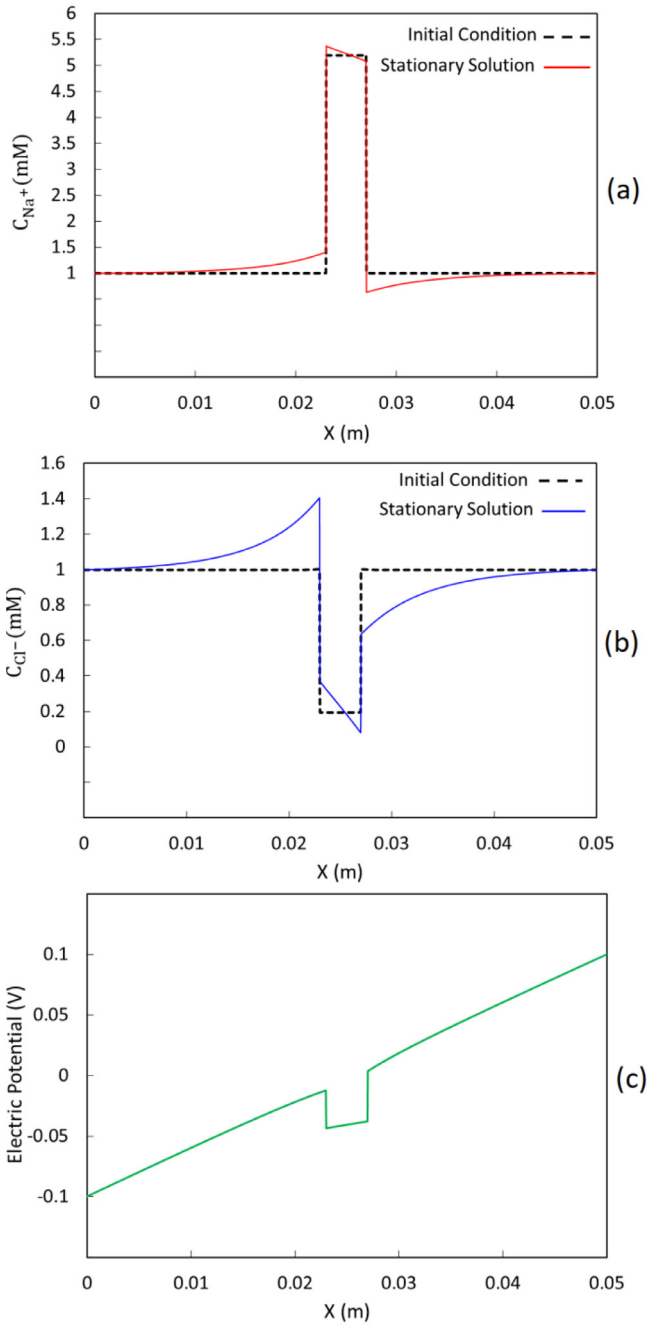

Fig. A.2. Initial (dashed lines) and stationary solution (solid lines) of concentrations of (a) sodium and (b) chloride ions. (c) The distribution of electric potential in the stationary state. All graphs are plotted at y = 0.025 m.

Table A2
Initial conditions and boundary conditions of the numerical model [45].

Initial Conditions		Boundary Conditions	
Inside Solution	Inside Gel	Anode	Cathode
$C_{Na^+} = 1$mM $C_{Cl^-} = 1$mM	$C_{Na^+} = 5.193$mM $C_{Cl^-} = 0.193$mM $C_{fixed} = 5$mM	$\phi = 0.1$V $C_{Na^+} = 1$mM $C_{Cl^-} = 1$mM	$\phi = -0.1$V $C_{Na^+} = 1$mM $C_{Cl^-} = 1$mM

$c_{Na+} = c_{Cl^-} = 1$ mM with a prescribed electric potential of -0.1V near the cathode and of +0.1V near the anode. The model parameters and boundary conditions are listed in Table A1 and Table A2.Fig. A.1 gives the concentrations of mobile species along with the electric voltage in the domain at initial and stationary states. The initial conditions and stationary solutions are presented in Fig. A.2. The results shown in Figs. A.1 and A.2 match very well with those presented in Wallmersperger et al.'s work [45].

Appendix B

We preformed mesh convergence analysis to ensure that the numerical results were independent of the number of elements and time steps. For this purpose, we considered the behavior of the scleral strips subjected to an electric potential of 10 V. The model parameters are given in Section 2.2 and the computational domain is shown in Fig. 2. The relative error $R_{error}$is computed using

$$R_{error} = \frac{\left\| c^{max}_{Na^+,i+1} - c^{max}_{Na^+,i} \right\|}{\left\| c^{max}_{Na^+,i+1} \right\|}$$

where $c^{max}_{Na^+,i}$ and $c^{max}_{Na^+,i+1}$ are the maximum ion concentrations obtained either from two consecutive mesh refinements when the time step is kept constant or from two consecutive time step refinements when the number of elements is kept constant. The relative error for the mechanical field equations was calculated using the maximum displacement of the free end of the strips. Fig. B1 shows that the relative errors reduce as the number of elements increases and the time stepdecreases.

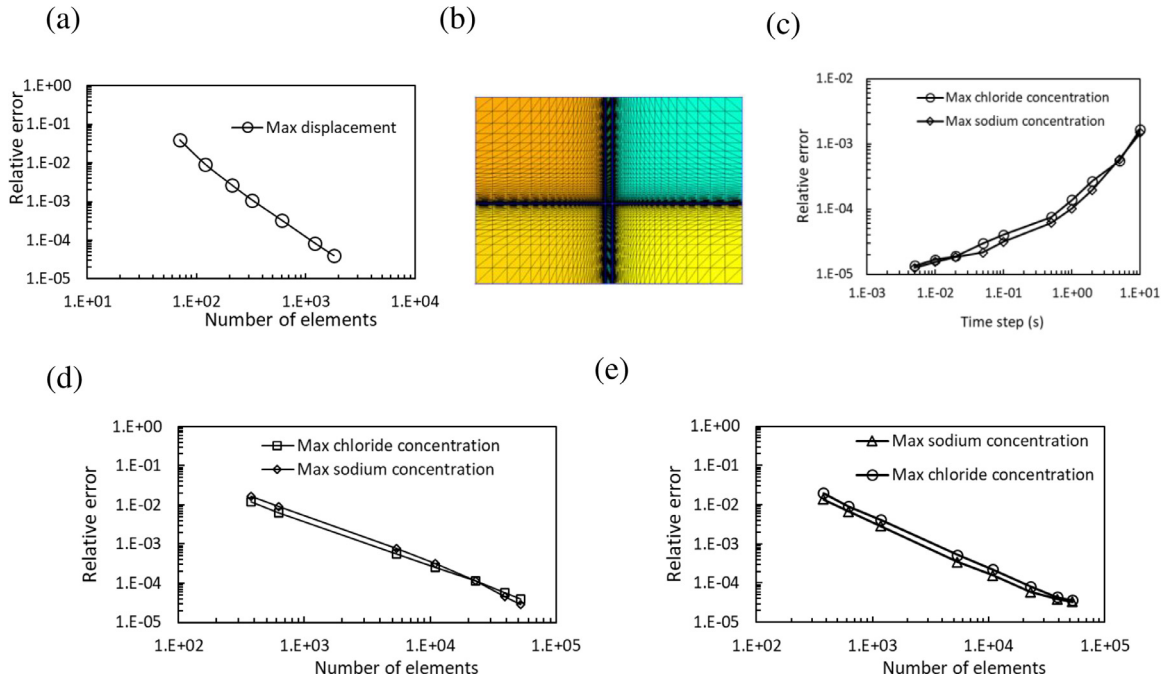

Fig. B1. (a) The effect of number of elements on the relative error computed based on the maximum displacement of strips. (b) The discretization of the computational domain that was used to solve the PNP equations in this work. c) The effect of time step on the relative error in the nonlinear coupled Poisson-Nernst-Planck system computed based on the maximum ionic concentration inside the domain using the mesh shown in (b). The effect of number of elements on the relative error in the PNP system when time steps of d) 1 s and e) 0.01 s were used.

References

[1] C. Boote, I.A. Sigal, R. Grytz, Y. Hua, T.D. Nguyen, M.J.A. Girard, Scleral structure and biomechanics, Prog. Retin. Eye Res. 74 (2020) 100773.
[2] I.C. Campbell, B. Coudrillier, C.Ross Ethier, Biomechanics of the posterior eye: a critical role in health and disease, J. Biomech. Eng. 136 (2) (2014) 021005.
[3] J.A. Rada, S. Shelton, T.T. Norton, The sclera and myopia, Exp. Eye Res. 82 (2) (2006) 185–200.
[4] M. Breen, R.L. Johnson, R. Sittig, H. Weinstein, A. Veis, The acidic glycosaminoglycans in human fetal development and adult life: cornea, sclera and skin, Connect. Tissue Res. 1 (4) (1972) 291–303.
[5] J.R. Dunlevy, J.A.S. Rada, Interaction of lumican with aggrecan in the aging human sclera, IOVS 45 (11) (2004) 3849–3856.
[6] J.A. Rada, V.R. Achen, C.A. Perry, P.W. Fox, Proteoglycans in the human sclera. Evidence for the presence of aggrecan, IOVS 38 (9) (1997) 1740–1751.
[7] T.R. Friberg, J.W. Lace, A comparison of the elastic properties of human choroid and sclera, Exp. Eye Res. 47 (3) (1988) 429–436.
[8] H. Hatami-Marbini, M. Pachenari, The contribution of sGAGs to stress-controlled tensile response of posterior porcine sclera, Plos One 15 (2) (2020) e0227856.
[9] H. Hatami-Marbini, M. Pachenari, On influence of sulfated glycosaminoglycans on tensile properties of posterior sclera, Mech. Soft Mater. 2 (1) (2020) 1–10.
[10] H. Hatami-Marbini, M. Pachenari, Tensile viscoelastic properties of the sclera after glycosaminoglycan depletion, Curr. Eye Res. (2021) 1–10.
[11] H. Hatami-Marbini, E. Etebu, Hydration dependent biomechanical properties of the corneal stroma, Exp. Eye Res. 116 (2013) 47–54.
[12] H. Hatami-Marbini, Hydration dependent viscoelastic tensile behavior of cornea, Ann Biomed Eng 42 (8) (2014) 1740–1748.
[13] H. Hatami-Marbini, M. Pachenari, Hydration related changes in tensile response of posterior porcine sclera, J. Mech. Behav. Biomed. Mater. 104 (2020) 103562.
[14] H. Hatami-Marbini, Viscoelastic shear properties of the corneal stroma, J. Biomech. 47 (3) (2014) 723–728.
[15] B. Loret, F.M. Simões, Effects of the pH on the mechanical behavior of articular cartilage and corneal stroma, Int. J. Solids Struct. 47 (17) (2010) 2201–2214.
[16] P.N. Lewis, C. Pinali, R.D. Young, K.M. Meek, A.J. Quantock, C. Knupp, Structural interactions between collagen and proteoglycans are elucidated by three--dimensional electron tomography of bovine cornea, Structure 18 (2) (2010) 239–245.
[17] J.A. Rada, V.R. Achen, S. Penugonda, R.W. Schmidt, B.A. Mount, Proteoglycan composition in the human sclera during growth and aging, IOVS 41 (7) (2000) 1639–1648.
[18] G.F. Elliott, S.A. Hodson, Cornea, and the swelling of polyelectrolyte gels of biological interest, Rep. Prog. Phys. 61 (10) (1998) 1325.
[19] Y. Huang, K.M. Meek, Swelling studies on the cornea and sclera: the effects of pH and ionic strength, Biophys. J. 77 (3) (1999) 1655–1665.
[20] B. Loret, F.M. Simões, Effects of pH on transport properties of articular cartilages, Biomech. Model Mechanobiol. 9 (1) (2010) 45–63.
[21] S. Kim, C. Laschi, B. Trimmer, Soft robotics: a bioinspired evolution in robotics, Trends Biotechnol 31 (5) (2013) 287–294.
[22] T. Mirfakhrai, J.D. Madden, R.H. Baughman, Polymer artificial muscles, Mater. Today 10 (4) (2007) 30–38.
[23] J.-M. Pernaut, J.R. Reynolds, Use of conducting electroactive polymers for drug delivery and sensing of bioactive molecules. A redox chemistry approach, J. Phys. Chem. 104 (17) (2000) 4080–4090.
[24] N. Zhang, R. Li, L. Zhang, H. Chen, W. Wang, Y. Liu, T. Wu, X. Wang, W. Wang, Y. Li, Actuator materials based on graphene oxide/polyacrylamide composite hydrogels prepared by in situ polymerization, Soft Matter 7 (16) (2011) 7231–7239.
[25] S.K. De, N. Aluru, B. Johnson, W. Crone, D.J. Beebe, J. Moore, Equilibrium swelling and kinetics of pH-responsive hydrogels: models, experiments, and simulations, J. Microelectromech. Syst. 11 (5) (2002) 544–555.
[26] V.S.R.K. Chinthala, S.S. Mulay, A.B. Harish, Constitutive modeling of pH-sensitive hydrogel: multi-physics coupling of electromagnetics with mechanics and thermodynamics, Mech. Mater. 161 (2021) 104002.
[27] V.S.R.K. Chinthala, S.S. Mulay, M. Hegde, The buckling and deflection studies of micro-electro-mechanical column and beam structures containing fixed-charges, Mech. Mater. 150 (2020) 103560.
[28] L. Ionov, Hydrogel-based actuators: possibilities and limitations, Mater. Today 17 (10) (2014) 494–503.
[29] R. Hamlen, C. Kent, S. Shafer, Electrolytically activated contractile polymer, Nature 206 (4989) (1965) 1149–1150.
[30] T. Tanaka, I. Nishio, S.-T. Sun, S. Ueno-Nishio, Collapse of gels in an electric field, Science 218 (4571) (1982) 467–469.
[31] Y. Yew, T. Ng, H. Li, K. Lam, Analysis of pH and electrically controlled swelling of hydrogel-based micro-sensors/actuators, Biomed. Microdevices 9 (4) (2007) 487–499.
[32] J. Shang, Z. Shao, X. Chen, Chitosan-based electroactive hydrogel, Polymer 49 (25) (2008) 5520–5525.
[33] A. Grodzinsky, N. Shoenfeld, Tensile forces induced in collagen by means of electromechanochemical transductive coupling, Polymer 18 (5) (1977) 435–443.
[34] N.A. Shoenfeld, A.J. Grodzinsky, Contribution of electrodiffusion to the dynamics of electrically stimulated changes in mechanical properties of collagen membranes, Biopolymers 19 (2) (1980) 241–262.
[35] D. De Rossi, P. Parrini, P. Chiarelli, G. Buzzigoli, Electrically induced contractile phenomena in charged polymer networks: preliminary study on the feasibility of muscle-like structures, Trans. Am. Soc. Artif. Intern. Organs 31 (1985) 60–65.

[36] D.E. De Rossi, P. Chiarelli, G. Buzzigoli, C. Domenici, L. Lazzeri, Contractile behavior of electrically activated mechanochemical polymer actuators, ASAIO Trans. 32 (1) (1986) 157–162.
[37] Y. Osada, J. Gong, K. Sawahata, Synthesis, mechanism, and application of an electro-driven chemomechanical system using polymer gels, J. Macromol. Sci. A 28 (11-12) (1991) 1189–1205.
[38] J. Gong, T. Nitta, Y. Osada, Electrokinetic modeling of the contractile phenomena of polyelectrolyte gels. One-dimensional capillary model, J. Phys. Chem. 98 (38) (1994) 9583–9587.
[39] T. Shiga, T. Kurauchi, Deformation of polyelectrolyte gels under the influence of electric field, J. Appl. Polym. Sci. 39 (11-12) (1990) 2305–2320.
[40] T. Shiga, Y. Hirose, A. Okada, T. Kurauchi, Bending of poly(vinyl alcohol)–poly(sodium acrylate) composite hydrogel in electric fields, J. Appl. Polym. Sci. 44 (2) (1992) 249–253.
[41] P. Grimshaw, J. Nussbaum, A. Grodzinsky, M. Yarmush, Kinetics of electrically and chemically induced swelling in polyelectrolyte gels, J. Chem. Phys. 93 (6) (1990) 4462–4472.
[42] M. Doi, M. Matsumoto, Y. Hirose, Deformation of ionic polymer gels by electric fields, Macromolecules 25 (20) (1992) 5504–5511.
[43] S.K. De, N.R. Aluru, A chemo-electro-mechanical mathematical model for simulation of pH sensitive hydrogels, Mech. Mater. 36 (5-6) (2004) 395–410.
[44] M.J. Bassetti, A.N. Chatterjee, N.R. Aluru, D.J. Beebe, Development and modeling of electrically triggered hydrogels for microfluidic applications, J. Microelectromech. Syst. 14 (5) (2005) 1198–1207.
[45] T. Wallmersperger, B. Kröplin, R.W. Gülch, Coupled chemo-electro-mechanical formulation for ionic polymer gels—-numerical and experimental investigations, Mech. Mater. 36 (5-6) (2004) 411–420.
[46] D. Ballhause, T. Wallmersperger, Coupled chemo-electro-mechanical finite element simulation of hydrogels: I. Chemical stimulation, Smart Mater. Struct. 17 (4) (2008) 045011.
[47] R. Luo, H. Li, K. Lam, Coupled chemo-electro-mechanical simulation for smart hydrogels that are responsive to an external electric field, Smart Mater. Struct. 16 (4) (2007) 1185.
[48] P. Glazer, M. Van Erp, A. Embrechts, S. Lemay, E. Mendes, Role of pH gradients in the actuation of electro-responsive polyelectrolyte gels, Soft Matter 8 (16) (2012) 4421–4426.
[49] S.Y. Kim, H.S. Shin, Y.M. Lee, C.N. Jeong, Properties of electroresponsive poly (vinyl alcohol)/poly (acrylic acid) IPN hydrogels under an electric stimulus, J. Appl. Polym. Sci. 73 (9) (1999) 1675–1683.
[50] M.L. O'Grady, P.-I. Kuo, K.K. Parker, Optimization of electroactive hydrogel actuators, ACS Appl. Mater. Interfaces 2 (2) (2009) 343–346.
[51] J. Shang, Z. Shao, X. Chen, Electrical behavior of a natural polyelectrolyte hydrogel: chitosan/carboxymethylcellulose hydrogel, Biomacromolecules 9 (4) (2008) 1208–1213.
[52] A. Flavell, M. Machen, B. Eisenberg, J. Kabre, C. Liu, X. Li, A conservative finite difference scheme for Poisson–Nernst–Planck equations, J. Comput. Electron. 13 (1) (2014) 235–249.
[53] J.H. Chaudhry, J. Comer, A. Aksimentiev, L.N. Olson, A stabilized finite element method for modified Poisson-Nernst-Planck equations to determine ion flow through a nanopore, Commun. Comput. Phys. 15 (1) (2014) 93–125.
[54] A. Solbrå, A.W. Bergersen, J. Van Den Brink, A. Malthe-Sørenssen, G.T. Einevoll, G. Halnes, A Kirchhoff-Nernst-Planck framework for modeling large scale extracellular electrodiffusion surrounding morphologically detailed neurons, PLoS Comput. Biol. 14 (10) (2018) e1006510.
[55] H.P. Langtangen, K.-A. Mardal, Introduction to Numerical Methods for Variational Problems, (2016).
[56] A. Logg, K.-A. Mardal, G. Wells, Automated Solution of Differential Equations by the Finite Element method: The FEniCS Book, Springer Science & Business Media, 2012.
[57] W.Y. Gu, H. Yao, A.L. Vega, D. Flagler, Diffusivity of ions in agarose gels and intervertebral disc: effect of porosity, Ann. Biomed. Eng. 32 (12) (2004) 1710–1717.
[58] W. Liu, C.M. Collins, M.B. Smith, Calculations of B(1) distribution, specific energy absorption rate, and intrinsic signal-to-noise ratio for a body-size birdcage coil loaded with different human subjects at 64 and 128 MHz, Appl. Magn. Reson. 29 (1) (2005) 5–18.
[59] Y. Lanir, J. Seybold, R. Schneiderman, J. Huyghe, Partition and diffusion of sodium and chloride ions in soft charged foam: the effect of external salt concentration and mechanical deformation, Tissue Eng. 4 (4) (1998) 365–378.
[60] B.J. Murienne, J.L. Jefferys, H.A. Quigley, T.D. Nguyen, The effects of glycosaminoglycan degradation on the mechanical behavior of the posterior porcine sclera, Acta Biomater 12 (2015) 195–206.
[61] Y. Li, Y. Sun, Y. Xiao, G. Gao, S. Liu, J. Zhang, J. Fu, Electric field actuation of tough electroactive hydrogels cross-linked by functional triblock copolymer micelles, ACS Appl. Mater. Interfaces 8 (39) (2016) 26326–26331.
[62] I.C. Kwon, Y.H. Bae, S.W. Kim, Characteristics of charged networks under an electric stimulus, J. Polym. Sci. B 32 (6) (1994) 1085–1092.
[63] M. Block, J. Kitchener, Polarization phenomena in commercial ion-exchange membranes, J. Electrochem. Soc. 113 (9) (1966) 947–953.
[64] R. Simons, Water splitting in ion exchange membranes, Electrochim. Acta 30 (3) (1985) 275–282.
[65] J. Battaglioli, R. Kamm, Measurements of the compressive properties of scleral tissue, IOVS 25 (1) (1984) 59–65.
[66] B. Loret, F.M. Simões, Biomechanical Aspects of Soft Tissues, CRC Press, Boca Raton, 2017.
[67] M.S. Borcherding, L. Blacik, R. Sittig, J.W. Bizzell, M. Breen, H. Weinstein, Proteoglycans and collagen fibre organization in human corneoscleral tissue, Exp. Eye Res. 21 (1) (1975) 59–70.
[68] J.V. Forrester, A.D. Dick, P. McMenamin, W. Lee, The eye, Basic Sci. Pract. (1996).
[69] B.K. Pierscionek, M. Asejczyk-Widlicka, R.A. Schachar, The effect of changing intraocular pressure on the corneal and scleral curvatures in the fresh porcine eye, Br. J. Ophthalmol. 91 (6) (2007) 801–803.
[70] A. Elsheikh, B. Geraghty, D. Alhasso, J. Knappett, M. Campanelli, P. Rama, Regional variation in the biomechanical properties of the human sclera, Exp. Eye Res. 90 (5) (2010) 624–633.
[71] J. Chen, G. Ma, Modelling deformation behaviour of polyelectrolyte gels under chemo-electro-mechanical coupling effects, Int. J. Numer. Methods Eng. 68 (10) (2006) 1052–1071.
[72] A. Attaran, J. Brummund, T. Wallmersperger, Modeling and simulation of the bending behavior of electrically-stimulated cantilevered hydrogels, Smart Mater. Struct. 24 (3) (2015) 035021.
[73] H. Li, Z. Yuan, K. Lam, H. Lee, J. Chen, J. Hanes, J. Fu, Model development and numerical simulation of electric-stimulus-responsive hydrogels subject to an externally applied electric field, Biosens. Bioelectron. 19 (9) (2004) 1097–1107.
[74] B. Cooke, Concentration polarization in electrodialysis—I. The electrometric measurement of interfacial concentration, Electrochim. Acta 3 (4) (1961) 307–317.
[75] M. Pachenari, H. Hatami-Marbini, Regional differences in the glycosaminoglycan role in porcine scleral hydration and mechanical behavior, IOVS 62 (3) (2021) 28.
[76] M.J. Girard, J.C. Downs, C.F. Burgoyne, J.-K.F. Suh, Peripapillary and posterior scleral mechanics—Part I: Development of an anisotropic hyperelastic constitutive model, J. Biomech. Eng. 131 (5) (2009) 051011.
[77] N.-J. Jan, K. Lathrop, I.A. Sigal, Collagen architecture of the posterior pole: high-resolution wide field of view visualization and analysis using polarized light microscopy, IOVS 58 (2) (2017) 735–744.
[78] G.A. Alyahya, S.M. Ribel-Madsen, S. Heegaard, J.U. Prause, K. Trier, Melanoma-associated spongiform scleropathy: biochemical changes and possible relation to tumour extension, Acta Ophthalmol. Scand. 81 (6) (2003) 625–629.
[79] T.T. Norton, J.A. Rada, Reduced extracellular matrix in mammalian sclera with induced myopia, Vision Res. 35 (9) (1995) 1271–1281.